Appl. Math. Mech. -Engl. Ed., **42**(2), 235–250 (2021)

APPLIED MATHEMATICS AND MECHANICS (ENGLISH EDITION)

https://doi.org/10.1007/s10483-021-2699-6

Quench characteristics and mechanical responses during quench propagation in rare earth barium copper oxide pancake coils*

Mengdie NIU[1,2], Jing XIA[3], Huadong YONG[1,2,†], Youhe ZHOU[1,2]

1. Key Laboratory of Mechanics on Disaster and Environment in Western China, The Ministry of Education of China, Lanzhou University, Lanzhou 730000, China;
2. Department of Mechanics and Engineering Sciences, College of Civil Engineering and Mechanics, Lanzhou University, Lanzhou 730000, China;
3. Institute of Applied Physics and Computational Mathematics, Beijing 100094, China;

(Received Aug. 23, 2020 / Revised Nov. 16, 2020)

Abstract Quench and mechanical behaviors are critical issues in high temperature superconducting (HTS) coils. In this paper, the quench characteristics in the rare earth barium copper oxide (REBCO) pancake coil at 4.2 K are analyzed, and a two-dimensional (2D) axisymmetric electro-magneto-thermal model is presented. The effects of the constituent materials, background field, and coil size are analyzed. An elastoplastic mechanical model is used to study the corresponding mechanical responses during the quench propagation. The variations of the temperature and strain in superconducting layers are compared. The results indicate that the radial strain evolutions can reflect the transverse quench propagation and the tensile hoop and radial stresses in superconducting layers increase with the quench propagation. The possible damages are discussed with the consideration of the effects of the background field and coil size. It is concluded that the high background field significantly increases the maximum tensile hoop and radial stresses in quenching coils and local damage may be caused.

Key words rare earth barium copper oxide (REBCO) pancake coil, hoop stress, quench characteristic, mechanical response, radial stress

Chinese Library Classification O34
2010 Mathematics Subject Classification 74B05, 74C05, 74S05

1 Introduction

Nowadays, rare earth barium copper oxide (REBCO) coated conductors have become the dominant practical conductors for high temperature superconducting (HTS) coils owing to their advanced current carrying capability and mechanical strength. In general, REBCO coils

* Citation: NIU, M. D., XIA, J., YONG, H. D., and ZHOU, Y. H. Quench characteristics and mechanical responses during quench propagation in rare earth barium copper oxide pancake coils. *Applied Mathematics and Mechanics* (*English Edition*), **42**(2), 235–250 (2021) https://doi.org/10.1007/s10483-021-2699-6

† Corresponding author, E-mail: yonghd@lzu.edu.cn

Project supported by the National Natural Science Foundation of China (Nos. 11872195, 11472120, and 11802036) and the 111 Project (No. B14044)

operate under complicated conditions with low ambient temperature and high background field for the generation of strong central magnetic field[1]. Under such conditions, coils are relatively susceptible to unexpected mechanical and thermal disturbances, i.e., conductor motion, non-recoverable local defects, heat leakage, and failure of the cryogenic system[2]. Quench and mechanical issues are of vital importance to HTS coils and high field magnets[3–4].

In HTS systems, the quench characterization is relatively complicated. In addition to the quench propagation in the longitudinal direction, the transverse quench propagation should be thoroughly studied. Sumption et al.[5] experimentally investigated the quench properties of REBCO coils, and concluded that the transverse normal zone propagation velocity (V_{NZP}) was one or two orders of magnitude smaller than the longitudinal V_{NZP}. They also pointed out that increasing the transverse V_{NZP} could compensate the longitudinal one and then facilitate the quench detection and protection. Many efforts have been made to increase the V_{NZP} or thermal stability of HTS coils by modifying the cooling pattern[6] and constituent materials[7–10], among which partial insulation, metal-as-insulation winding, and no-insulation (NI) technology play a significant role on improving the self-protection property of HTS coils, even though they could result in charging delay or field drift issues. In quench analyses, two-dimensional (2D) and three-dimensional (3D) quench models have been established for coils[7] and conductors on round core (CORC) cables[11], respectively. Recently, Pi et al.[12] developed a four-dimensional (4D) quench model to study the quench behavior of quasi-isotropic superconducting cables.

During quench propagation, it is noteworthy that non-negligible thermal stress and strain will be generated due to the thermal mismatch between constituent materials. Under such thermal stress and high Lorentz force under high filed conditions, the mechanical issues in the process of quench propagation should be concerned. The reasons are that, the electrical properties of the REBCO conductor can be affected by mechanical deformation and stress[13], and the current-carrying capacity might drop severely if the tensile stress and strain exceed the corresponding irreversible limits[14]. Besides, the possible delamination will occur between the constituent layers of the conductor after the tensile transverse stress exceeds the critical one[15]. In addition, severe degradation can be caused, and the possible mechanical damage should be cared[16].

A simple analytic formula,

$$\sigma_\varphi = rJ_\varphi B_z$$

in which r, J_φ, B_z, and σ_φ denote the radius, the current density, the axial magnetic field, and the hoop stress, respectively, gives a rough estimation on the hoop stress induced by the Lorentz force. A more complex analytical formula[17] originates from the classic elastic theory, in which the coil is reduced to a disk and the plane stress approximation is adopted. Arp[18] summarized analytical formulae for calculating the stress and strain in superconducting solenoids due to winding, cooling, and magnetic forces. Numerical analyses based on the combined homogenous cylinder model[19] or continuum bulk model[20–21] are often used in coil stress calculation. Xia et al.[22] analyzed the screening current effect on the stress and strain in HTS magnets, and compared the results obtained by the continuum bulk model and the discrete contact model.

However, most of the aforementioned mechanical models adopted linearly elastic approximations, and the composite coated conductor was treated as homogenous with a mixed rule. Under the action of large load, linearly elastic approximation can cause non-negligible estimation bias since high stress is very likely to cause plastic deformation in the tape. Therefore, it is necessary to establish an elastoplastic mechanical model for more exact estimation of stress and strain in REBCO pancake coils. In this paper, the quench and mechanical behaviors in REBCO pancake coils at 4.2 K are numerically analyzed. The electro-magneto-thermal model and elastoplastic mechanical model are used and presented in Section 2. In Section 3, the quench behaviors of REBCO pancake coils and the effects of the constituent materials, external field, and coil inner radius are obtained and compared. In Section 4, the variations of stress

and strain in the quenching coils are evaluated. Finally, the conclusions are given in Section 5.

2 Numerical models

The object in our simulation is single insulated pancake coils with the turn number of 100, fabricated by co-winding REBCO coated conductor from SuperPower Inc. and Kapton tape. Coated conductor is mainly composed of copper stabilizer layers, substrate, and REBCO layers. In modeling, to speed up calculation, most of the constituent layers are considered while the silver and buffer layers are omitted. Considering the axis-symmetry property of the pancake coil, a reduced 2D axisymmetric model is established with the actual size and configurations shown in Fig. 1, where the coil inner and outer radii are 30 mm and 40 mm, respectively, the height is 4 mm, and the thicknesses of copper, substrate, REBCO, and Kapton are 20 μm, 50 μm, 1 μm, and 59 μm, respectively.

In the simulation, to trigger the quench in REBCO pancake coils, the heat power is uniformly exerted on the partial insulation layer of the 50th turn for 50 ms. In order to monitor the quench initiation and propagation, several temperature and strain probes are regularly arranged on the superconducting layers near the heat region, as shown in Fig. 1. The simulation here focuses on the transverse quench propagation, and the longitudinal one cannot be described. In that case, 3D modeling is needed, which is not yet within the scope of our analysis. In the following, we will introduce the quench and mechanical models in detail.

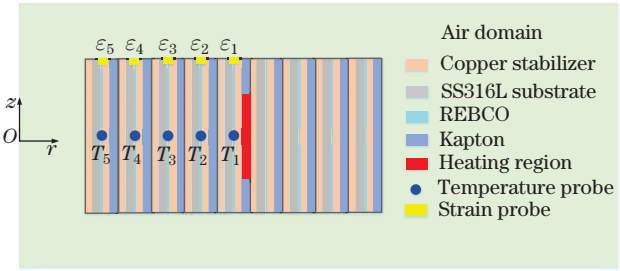

Fig. 1 Model diagram of the REBCO pancake coil, in which nine turns near the heat region are drawn for clear vision. The heat region is located at the partial insulation layer of the middle turn with the cross-sectional area of 0.4 mm×0.059 mm, and the temperature and strain probes are arranged sequentially on superconducting layers (color online)

2.1 Electromagnetic model based on H-formulation

In this subsection, we calculate the electromagnetic field distribution of REBCO pancake coils with the aid of H-formulation[23] and *E*-*J* power law. The governing equations of H-formulation are written as follows:

$$\frac{\partial\left(r\rho\left(\frac{\partial H_r}{\partial z}-\frac{\partial H_z}{\partial r}\right)\right)}{\partial z}=\mu_0 r\frac{\partial H_r}{\partial t},\quad -\frac{\partial\left(r\rho\left(\frac{\partial H_r}{\partial z}-\frac{\partial H_z}{\partial r}\right)\right)}{\partial r}=\mu_0 r\frac{\partial H_z}{\partial t}, \tag{1}$$

where H_r and H_z are the radial and axial magnetic fields in the 2D axisymmetric model, respectively. μ_0 refers to the permeability of vacuum ($\mu_0 = 4\pi \times 10^{-7}\,\mathrm{T\cdot m\cdot A^{-1}}$). The electric resistivity ρ is temperature-dependent except for air domains and insulation layers, whose resistivity values are given as $1\,\Omega\cdot\mathrm{m}$ for fast convergence. The resistivity values of copper[24], stainless steel[24], and Hastelloy[25] are illustrated in Fig. 2(a). The resistivity of the superconducting layer can be calculated from the *E*-*J* power law as follows:

$$E_\varphi = E_0\frac{J_\varphi}{J_c}\left|\frac{J_\varphi}{J_c}\right|^{n-1}, \tag{2}$$

where E_φ is the electric field, and E_0 is the reference electric field with a value of $1\times10^{-4}\,\mathrm{V\cdot m^{-1}}$. J_φ is the current density, and J_c is the critical current density depending on the magnetic field and temperature. The power index n is 31[26]. Here, a conventional elliptical formula[26] is introduced to describe the angular dependence of the critical current I_c on the magnetic flux density for the REBCO tape at 4.2 K.

$$I_\mathrm{c}(\boldsymbol{B},\theta)=I_\mathrm{c}(B_r,B_z)=I_{\mathrm{c}0}\Big(1+\frac{\sqrt{((aB_z)^2+B_r^2)}}{B_\mathrm{c}}\Big)^{-b}, \tag{3}$$

where[26–27]

$$I_{\mathrm{c}0}=720\,\mathrm{A},\quad a=0.038\,13,\quad B_\mathrm{c}=0.631\,\mathrm{T},\quad b=0.712\,2.$$

To illustrate the correlation between the critical current and the temperature, a typical model described in Ref. [11] is adopted:

$$I_\mathrm{c}(T)=\begin{cases} I_\mathrm{c}(B_r,B_z)\Big(\dfrac{T_\mathrm{c}-T}{T_\mathrm{c}-T_0}\Big)^{\beta}, & T_0\leqslant T<T_\mathrm{c},\\ 0, & T\geqslant T_\mathrm{c}, \end{cases} \tag{4}$$

where β represents the temperature dependence of the critical current, ranging from 1 to 2. Here, the nonlinear relationship between the critical current and the temperature is simplified and $\beta=1$ is chosen for the quench simulation[26]. By substituting the relation in Eq. (4) into Eq. (2), one can find that the resistivity of the superconducting layer becomes infinitely large when $T\geqslant T_\mathrm{c}$ ($T_\mathrm{c}=92\,\mathrm{K}$). This phenomenon is unreasonable, as the superconductor would be locally transformed into the normal conductor for $T\geqslant T_\mathrm{c}$. Therefore, a modified formula[28] is introduced to fit the smooth transition of the electric resistivity $\widetilde{\rho}_\mathrm{sc}$ in the superconducting layer, i.e.,

$$\widetilde{\rho}_\mathrm{sc}=\frac{\rho_\mathrm{sc}\rho_\mathrm{n}}{\rho_\mathrm{sc}+\rho_\mathrm{n}}, \tag{5}$$

where ρ_sc is the resistivity of the superconducting layer in the superconducting state, ρ_n is the corresponding resistivity in the normal state, and

$$\rho_\mathrm{sc}=\frac{E_0}{J_\mathrm{c}}\left|\frac{J_\varphi}{J_\mathrm{c}}\right|^{n-1},\quad \rho_\mathrm{n}=10^{-5}\,\Omega\cdot\mathrm{m}.$$

2.2 2D axisymmetric heat transfer model

The corresponding heat diffusion equation is given as follows:

$$\upsilon c_p\frac{\partial T}{\partial t}=\Big(\frac{1}{r}\frac{\partial(rk\frac{\partial T}{\partial r})}{\partial r}+\frac{\partial(k\frac{\partial T}{\partial z})}{\partial z}\Big)+Q_p+Q_s, \tag{6}$$

where υ, c_p, and k represent the mass density, the specific heat capacity, and the thermal conductivity, respectively. The temperature dependence of c_p and k is considered and plotted in Figs. 2(b) and 2(c), respectively. Q_p is the heating power, and Q_s stands for the Joule heat ($Q_s=E\cdot J$). It is assumed that the boundary of REBCO coils is adiabatic and a uniform temperature distribution ($T_0=4.2\,\mathrm{K}$) inside the winding is set as the initial condition.

2.3 Elastoplastic mechanical model

A 2D-axisymmetic elastoplastic mechanical model is implemented in the finite element method (FEM) software for the stress-strain calculation of coils during the quench propagation. The electromagnetic load and temperature change are considered. For simplicity, the magnetic

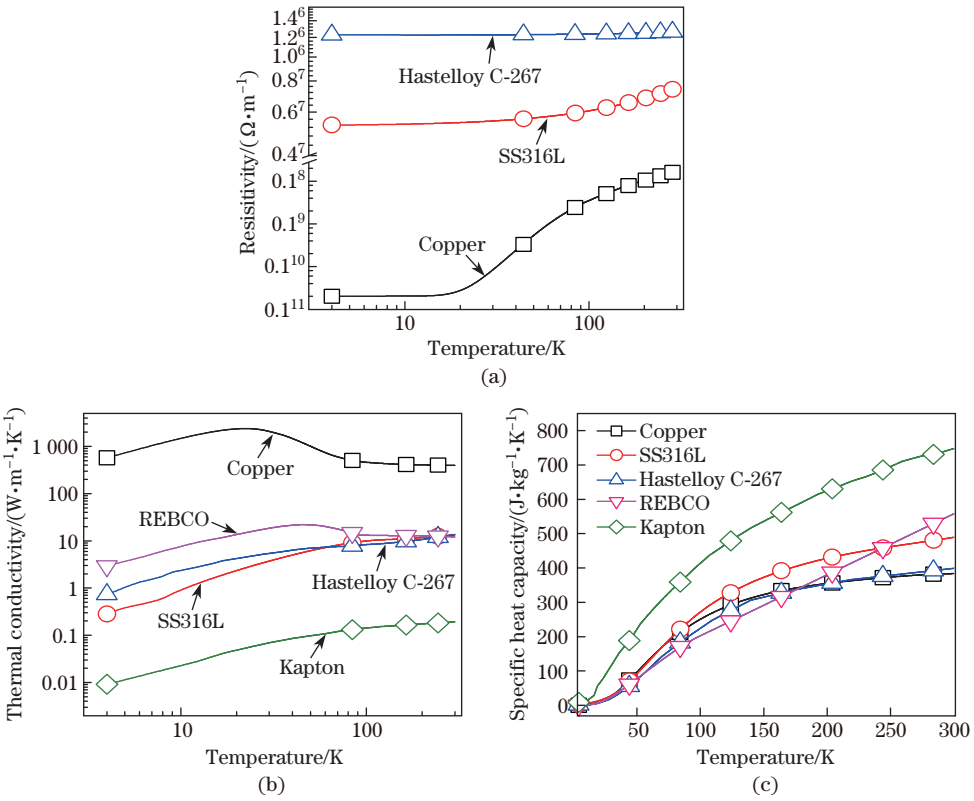

Fig. 2 Resisitivity, thermal conductivity, and specific heat capacity of constituent materials[24–25, 29–31] (color online)

field change and heat generation caused by structural deformation are not taken into account in the simulation.

Here, the constituent materials inside the winding are considered to be continuous, isotropic, elastic, or elastoplastic. The mechanical model is assumed to have small deformation, and the geometric nonlinearity can be neglected. The pancake coil is considered to be placed between two rigid plates, and the displacements of the upper and bottom edges in the axial direction are set as zero. All layers inside the coils are assumed to be bonded together, and the radial and shear stresses on the inner and outer boundaries of coils are zero.

In the mechanical analysis, the electromagnetic force and the temperature change induced by the quench propagation are applied gradually. At each load increment, the structural equilibrium is satisfied. The mechanical equilibrium equations in the 2D axisymmetric model are

$$\frac{\partial \sigma_r}{\partial r}+\frac{\partial \tau_{zr}}{\partial z}+\frac{\sigma_r-\sigma_\varphi}{r}+f_r=0,\quad \frac{\partial \sigma_z}{\partial z}+\frac{\partial \tau_{rz}}{\partial r}+\frac{\tau_{rz}}{r}+f_z=0, \tag{7}$$

where σ_r, σ_φ, σ_z, and τ_{rz} are the non-zero components of the stress tensor. The body forces f_r and f_z represent the radial and axial electromagnetic forces, respectively, $f_r=B_zJ_\varphi$, and $f_z=-B_rJ_\varphi$. For the brittle material like the REBCO layer, a linearly elastic behavior approximation is adopted, and the generalized Hooke's law[32] is applicable in the description of the stress-strain relationship as follows:

$$\begin{pmatrix}\sigma_r\\ \sigma_\varphi\\ \sigma_z\\ \tau_{zr}\end{pmatrix}=\begin{pmatrix}\lambda+2G & \lambda & \lambda & 0\\ \lambda & \lambda+2G & \lambda & 0\\ \lambda & \lambda & \lambda+2G & 0\\ 0 & 0 & 0 & G\end{pmatrix}\begin{pmatrix}\varepsilon_r-\varepsilon_{\rm th}\\ \varepsilon_\varphi-\varepsilon_{\rm th}\\ \varepsilon_z-\varepsilon_{\rm th}\\ \gamma_{zr}\end{pmatrix}, \tag{8}$$

where ε_r, ε_φ, ε_z, and γ_{zr} denote the non-zero components of the total strain tensor. $\varepsilon_{\rm th}$ is the thermal strain induced by the temperature change, and $\varepsilon_{\rm th}=\alpha(T-T_0)$ in which α is the thermal expansion coefficient. λ and G are Lamé's constants, $\lambda=\mu E/((1+\mu)(1-2\mu))$, and $G=E/(2(1+\mu))$, in which E and μ represent the elastic modulus and Poisson's ratio, respectively. The corresponding parameters are listed in Table 1. The geometric equations in the 2D axisymmetric model are expressed as follows:

$$\varepsilon_r=\frac{\partial u}{\partial r},\quad \varepsilon_\varphi=\frac{u}{r},\quad \varepsilon_z=\frac{\partial w}{\partial z},\quad \gamma_{zr}=\frac{\partial w}{\partial r}+\frac{\partial u}{\partial z}, \tag{9}$$

where u and w denote the displacements in the radial and axial directions, respectively.

However, for the elastoplastic material like copper stabilizers, Eq. (8) is not applicable when yielding occurs. The elastoplastic constitutive relation needs to be established. A small plastic strain model is assumed, and the total strain tensor $\boldsymbol{\varepsilon}$ can be additively decomposed into the elastic strain tensor $\boldsymbol{\varepsilon}_{\rm el}$, the plastic strain tensor $\boldsymbol{\varepsilon}_{\rm pl}$, and the thermal strain tensor $\boldsymbol{\varepsilon}_{\rm th}$[32].

$$\boldsymbol{\varepsilon}=\boldsymbol{\varepsilon}_{\rm el}+\boldsymbol{\varepsilon}_{\rm pl}+\boldsymbol{\varepsilon}_{\rm th}. \tag{10}$$

We use the von Mises yield criterion[32] to determine whether the material yields. The bilinear isotropic hardening law[32–33] is also adopted. It can be described by

$$\sigma_{\rm ys}=\sigma_{\rm ys0}+\frac{E_{\rm t}E}{E-E_{\rm t}}\varepsilon_{\rm ep}, \tag{11}$$

where $\sigma_{\rm ys0}$ is the initial yield strength, $E_{\rm t}$ and $\varepsilon_{\rm ep}$ are the tangent module and the effective plastic strain, respectively.

Table 1 Properties of constituent materials in REBCO pancake coils[24, 34–38]

Property	Copper	Stainless steel	REBCO	Kapton
Mass density ν/(kg·m^{-3})	8 940	8 000	5 900	1 420
Thermal expansion coefficient $\alpha\times10^{-6}$/(K^{-1})	14	12.7	11	20
Elastic modulus E/GPa	85	193	150	3
Poisson's ratio μ	0.338	0.3	0.3	0.34
Yield strength $\sigma_{\rm ys0}$/MPa	350	840	–	69
Tangent modulus $E_{\rm t}$/GPa	4	10	–	1

3 Simulation results on the quench behavior of REBCO pancake coils

3.1 Quench behavior of REBCO pancake coils

Two important quench characterized parameters in REBCO pancake coils, i.e., the minimum quench energy $E_{\rm MQ}$ (unit: J) and the transverse $V_{\rm NZP}$ (unit: mm·s^{-1}) are introduced and defined as follows:

$$E_{\rm MQ}=\int_{V_{\rm heater}}t_{\rm h}Q_{\rm mp}{\rm d}V,\quad V_{\rm NZP}=\frac{\Delta w}{\Delta t}, \tag{12}$$

in which $V_{\rm heater}$ is the volume of the heating region, $t_{\rm h}$ is the heating time, $t_{\rm h} = 50\,{\rm ms}$, and $Q_{\rm mp}$ is the minimum heating power required to initiate the quench propagation in the coil. Δt represents the time delay that occurs when the adjacent superconducting layers reach the critical temperature, and Δw is the corresponding radial spacing.

First, the critical currents of REBCO pancake coils at self-field and external field cases are calculated by using the self-consistent model[39–40]. The critical currents at self-field and in-field cases are labeled as $I_{\rm c0,coil}$ and $I_{\rm c,coil}(B_{\rm ext})$, respectively, where $B_{\rm ext}$ is the external field.

Then, the minimum quench energy of the pancake coil is analyzed by modifying the magnitude of heating power. With the accumulation of heat, quench first occurs in the superconducting layer closer to the heating region, and the temperature of Probe T_1 can be regarded as the hot-spot temperature $T_{\rm hot}$. Figure 3(a) plots the hot-spot temperature in coils with the transporting current of 333 A ($0.8I_{\rm c0,coil}$). It is found that once the heating energy slightly exceeds 3.85 J, the hot-spot temperature increases to exceed the critical temperature after the heat pulse, and then quench occurs. Thus, $E_{\rm MQ}$ in such cases can be determined as 3.85 J.

At the heating energy of 3.85 J, the current transfer between layers occurs in the 50th turn, closer to the heating area. The current redistribution is shown in Fig. 3(b). The heating power input causes the hot-spot temperature to increase beyond the current sharing temperature, and thus part of the operating current in the superconducting layers flows into the copper layers. After the heat pulse, the hot-spot temperature and current distribution nearly remain unchanged in a short period of 1 s, which is not drawn in Fig. 3(b). Immediately after this, the hot-spot temperature climbs, and the current in the superconducting layers transfers into the copper layers, which is the consequence of the fact that the Joule heat in the copper layers cannot spread out by the thermal conduct. There is almost no transporting current in the superconducting layers when quench occurs ($T \geqslant T_{\rm c}$). Meanwhile, quench propagation starts, and the temperatures in adjacent superconducting layers rise rapidly, as plotted in Fig. 3(c). The temperatures in probes of T_1, T_2, T_3, and T_4 ascend in the similar trend. We can take the time delay between T_2 and T_4 as Δt. According to Eq. (12), $V_{\rm NZP}$ is approximately $9.4\,{\rm mm{\cdot}s^{-1}}$. It can be seen that the simulation result for $V_{\rm NZP}$ of REBCO coils at 4.2 K is close to the experimental results for a small YBCO coil at 4.2 K[41].

3.2 Factor analysis on quench behavior of REBCO pancake coils

In this subsection, we will study the influence of several practical factors on $E_{\rm MQ}$ and transverse $V_{\rm NZP}$. These factors include the substrate material, background field, and coil size of the REBCO pancake coil.

3.2.1 Substrate materials

Stainless steel and Hastelloy are conventional substrate materials in the manufacturing of REBCO coated conductors. Here, a detailed comparison on $E_{\rm MQ}$ and $V_{\rm NZP}$ of stainless steel-based coil and Hastelloy-based coil is presented in Fig. 4. From Fig. 4(a), we can see that the $E_{\rm MQ}$ values of both coils decrease with the increase in the normalized operating current i ($= I_0/I_{\rm c0,coil}$, where I_0 is the transporting current). At the range of normalized operating current from 0.6 to 0.8, $E_{\rm MQ}$ of stainless steel-based coil descends from 10 J to 4 J, and the counterpart of the Hastelloy-based coil reduces from 9.5 J to 3.5 J. The stainless steel-based coil has a higher $E_{\rm MQ}$ than the Hastelloy-based coil, and the discrepancy between their values of $E_{\rm MQ}$ is about 0.5 J. Such a difference is caused by the specific heat of stainless steel which is higher than that of Hastelloy at low-temperature region. However, $V_{\rm NZP}$ in the transverse direction shows an opposite tendency (see Fig. 4(b)). For the Hastelloy-based coil, the transverse $V_{\rm NZP}$ increases from $4\,{\rm mm{\cdot}s^{-1}}$ to $5.8\,{\rm mm{\cdot}s^{-1}}$ at the range of the normalized operating current from 0.6 to 0.8. Similarly, the counterpart in the stainless-steel based coil rises from $4.3\,{\rm mm{\cdot}s^{-1}}$ to $5.6\,{\rm mm{\cdot}s^{-1}}$ with the normalized operating current from 0.65 to 0.8, and this counterpart is slightly less than that of the Hastelloy-based coil. By comparison, we find that the stainless steel-based coil has higher $E_{\rm MQ}$ while its transverse $V_{\rm NZP}$ is comparatively

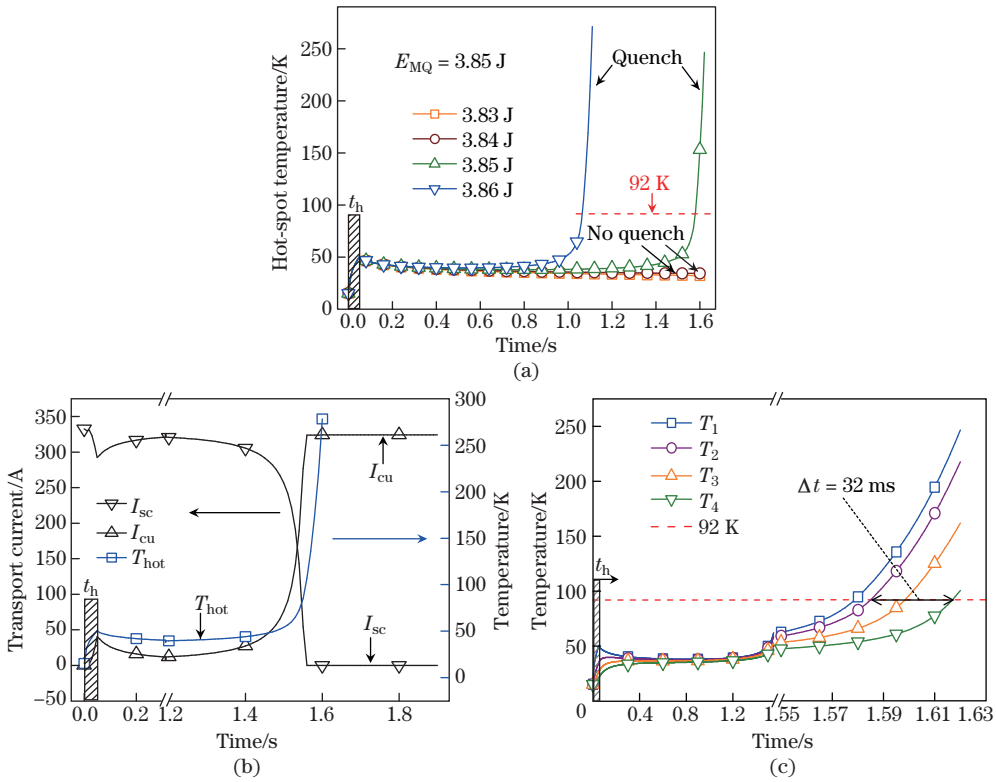

Fig. 3 (a) Hot-spot temperature T_{hot} ($= T_1$) in coils with the transporting current of 333 A under different heating energies; (b) current redistributions and (c) temperatures of Probes T_1, T_2, T_3, and T_4 in adjacent superconducting layers at the heating energy of 3.85 J (color online)

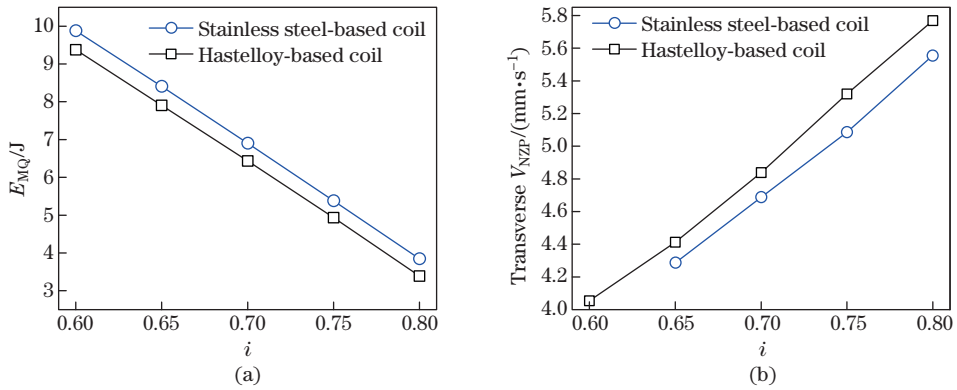

Fig. 4 (a) E_{MQ} versus the normalized operating current i for the stainless steel-based coil and Hastelloy-based coil; (b) the corresponding V_{NZP} in the transverse direction at the heating energy of 9.7 J (color online)

lower. Thus, the stainless steel-based coil will be further investigated in the following simulation.

3.2.2 Axial background field and coil size

High background field is demanded for the generation of a large central field in magnets. For this reason, we further discuss the quench behavior in pancake coils under different external fields. Figure 5 presents the normalized E_{MQ} and V_{NZP} of pancake coils with the normalized operating current i ($= I_0/I_{c,coil}(B_{ext})$) of 0.8 and various background fields. It can be seen that

E_{MQ} decreases slightly with increasing the background field when the background field exceeds 2.5 T. No decrease in E_{MQ} is found at the background field of 2.5 T, while it shows 12% decrease of E_{MQ} at the 15 T background field. The reason why E_{MQ} reduces is that the current sharing temperature is reduced by the high background field. Similar to the variation of E_{MQ}, V_{NZP} (at the heating energy of 3.85 J) also descends with the background field from 2.5 T to 15 T, which should be attributed to the decrease in the critical current and operating current. At a large background field of 15 T, the transverse V_{NZP} is 0.65 of the counterpart in the self-field case. Thus, high background field inevitably affects the transverse quench propagation.

The variations of E_{MQ} and V_{NZP} with the coil inner radius are shown in Fig. 6. From Fig. 6, we can see that E_{MQ} at the 0 T external field increases linearly from 2.8 J to 5.9 J with the coil inner radius from 20 mm to 50 mm. This is attributable to the increased heat capacity due to the increase in the coil inner radius. The similar rising tendency is also observed at the background field of 15 T, the corresponding E_{MQ} rises from 2.5 J to 5.2 J. In addition, the transverse V_{NZP} is almost unchanged with the coil inner radius from 20 mm to 50 mm for both the self-field and the 15 T background field cases. In other words, E_{MQ} is more sensitive to the variation of the coil size, whereas the transverse V_{NZP} is almost unaffected.

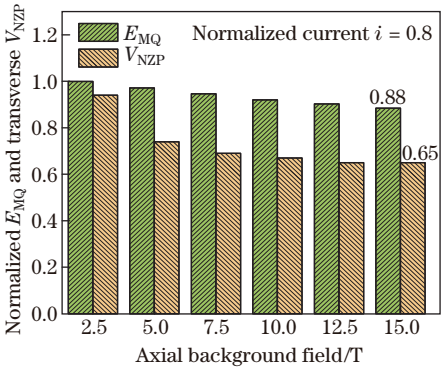

Fig. 5 Normalized E_{MQ} and transverse V_{NZP} versus the axial background field, where E_{MQ} and V_{NZP} are normalized by their counterparts in the self-field case (color online)

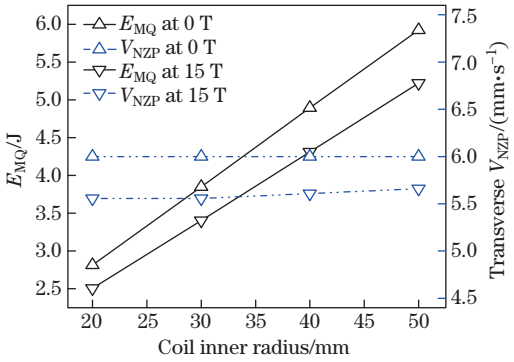

Fig. 6 E_{MQ} and transverse V_{NZP} of pancake coils with various coil inner radii and the normalized operating current of 0.8 (color online)

4 Mechanical responses of coils during quench propagation

4.1 Comparison of temperature and radial strain evolutions in superconducting layers

The mechanical responses of the pancake coil in the process of quench propagation are evaluated by using the aforementioned elastoplastic mechanical model. The quench detection technology based on strain evolutions has been proved to be useful in low temperature superconducting (LTS) structures[42–43], which inspires us to see if the strain variations can characterize the quench propagation in the HTS coil.

Figure 7 compares the variations of temperature and radial strain in the superconducting layers of coil with the operating current of 250 A ($0.6I_{c0,coil}$) and the heat power of 35.5 W·m^{-3}. We can see that the temperatures of Probes T_1–T_4 (see Fig. 7(a)) and the radial strains of Probes ε_1–ε_4 (as shown in Fig. 7(b)) in the superconducting layers rise in a similar trend after heat pulse. This reminds us that the radial strain evolutions can also reflect the transverse quench propagation in the REBCO pancake coil. Here, the reference radial strain 0.15% is selected to evaluate the transverse V_{NZP} due to the similar tendency among ε_1, ε_2, ε_3, and ε_4 as they exceed 0.15%.

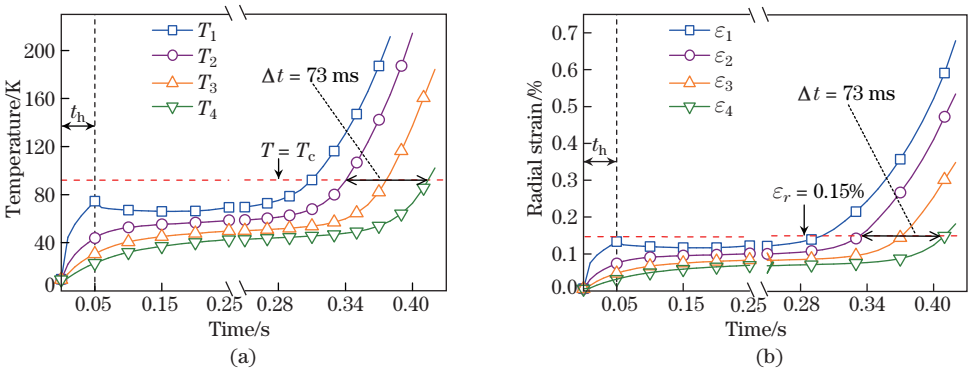

Fig. 7 (a) Temperatures of Probes T_1–T_4 and (b) radial strains of Probes ε_1–ε_4 in the superconducting layers of REBCO pancake coils with the operating current of 250 A and the heating power of 35.5 W·m^{-3} (color online)

The evaluated time delay between ε_2 and ε_4 is identical to the counterpart between T_2 and T_4. According to the definition of transverse V_{NZP} in Eq. (12), we can easily find that the values of V_{NZP} based on temperature and radial strain evolutions are consistent. Consequently, the theoretical feasibility of the strain-based quench detection technology for HTS coils is validated.

4.2 Stress-strain states of coils under high field conditions

In this subsection, the normalized operating current is 0.6, the heating power is 35.5 W·m^{-3}, and the heating duration is 50 ms. The stress-strain states of the pancake coil in the process of quench propagation will be evaluated and compared. Only the cases where T_{hot} is within 200 K are discussed to avoid critical thermal stress[44].

Figure 8 shows the contour plots of temperature T, radial stress σ_r, and hoop stress σ_φ in the quenching coil at the moment of T_{hot} = 200 K. One can see from Fig. 8 that the large temperature gradient in the radial direction resulting from lower V_{NZP} appears near the heating zone, and the temperature difference in the axial direction is almost zero. One can also see that the radial stresses in the inner turns are almost all at the tensile state and the radial stresses are at a compressive state for outer turns. The maximum tensile radial stress is 1.73 MPa in the case without external field, and it is increased to 6.03 MPa for the 5 T background field case. Different from the radial stress distribution, the hoop stress at the heat region shows a strong

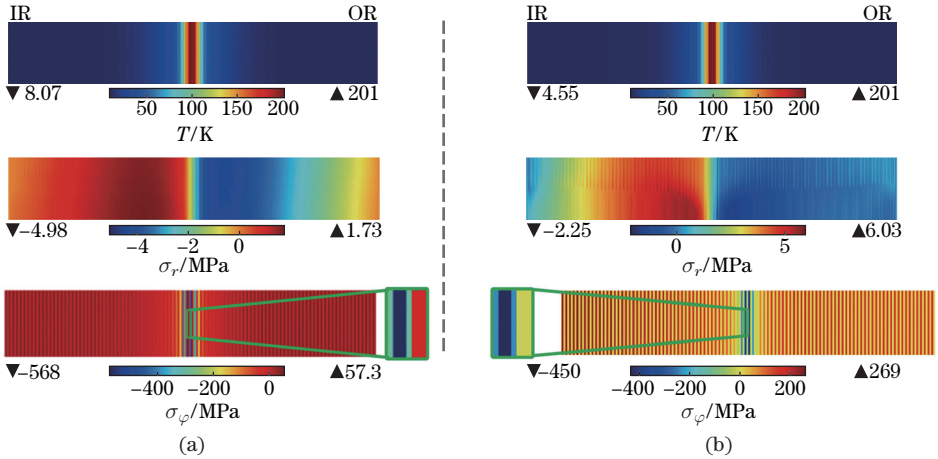

Fig. 8 Distributions of T, σ_r, and σ_φ in quenching coils at the moment of T_{hot} = 200 K for the coils with the axial background fields of (a) 0 T and (b) 5 T, where "IR" and "OR" represent the coil innermost region and the outermost region, respectively (color online)

discrepancy between the constituent layers, and the stainless steel substrate bears the maximum compressive hoop stress, which is −568 MPa at the self-field case and increases to −450 MPa for the 5 T background field case. No compressive hoop stress is found in the insulation layer. Furthermore, most of the tapes away from the heating region are subjected to the tensile hoop stress.

Figure 9 gives the variations of the hot-spot temperature, maximum hoop strain, peak hoop, and radial stresses in all superconducting layers. From Fig. 9(a), one can see that $T_{\rm hot}$ at the 10 T background field climbs to 200 K first due to the release of higher electromagnetic energy, and the counterpart at the 5 T external field reaches 200 K secondly. The maximum hoop strain gradually increases with the quench propagation. At the moment of $T_{\rm hot} = 200$ K, the maximum hoop strain reaches 0.23% for the 10 T external field, which is more than those for the 0 T and 5 T background fields.

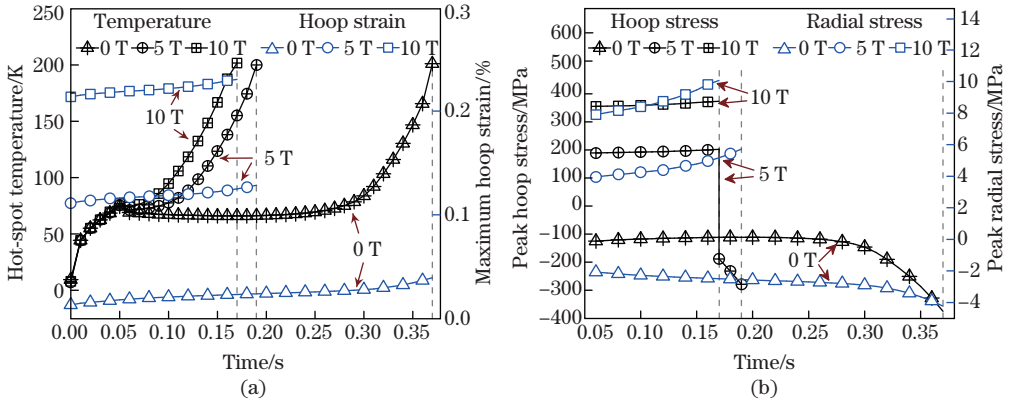

Fig. 9 Variations of (a) the hot-spot temperature and maximum hoop strain in the superconducting layers and (b) the peak hoop and radial stresses in the superconducting layers after the heat pulse for the coils with the axial background fields of 0 T, 5 T, and 10 T, where the vertical dashed lines represent the moment of $T_{\rm hot} = 200$ K (color online)

Similarly, the values of the peak hoop and radial stresses in the superconducting layers increase with the quench propagation, as shown in Fig. 9(b). For the case without external field, the peak hoop and radial stresses are all at the compressive state after the heat pulse, and are increased to −370 MPa and −4.2 MPa at the moment of $T_{\rm hot} = 200$ K, respectively. The stress distribution at the self-field case is mainly affected by the thermal stress due to the higher temperature rise and temperature gradient near the heat region, which can be seen in Fig. 8(a). For the cases with the background fields of 5 T and 10 T, the peak hoop and radial stresses are almost all at the tensile state because of the large radial Lorentz force of $J_\varphi \cdot B_z$. Notably, both the Lorentz force and the thermal stress can affect the stress distribution, and the $J_\varphi B_z r$ formula is not applicable for hoop stress calculation. The compressive stress dominates the peak hoop stress at the moment of $T_{\rm hot} = 200$ K for the 5 T external field case. At the moment of $T_{\rm hot} = 200$ K, the peak hoop stress in the superconducting layers at the 10 T external field ascends from 350 MPa to 370 MPa, and the corresponding peak tensile radial stress climbs from 7.9 MPa to 9.7 MPa. This enhancement mainly originates from the temperature change in the process of quench propagation.

In summary, the stress-strain states of quenching coils are affected by both the thermal stress and the Lorentz force. Accompanied by the quench propagation, the peak hoop and radial stresses are all at the compressive state for the self-field case, and they are almost all at the tensile state for the high background field case. The peak hoop and radial stresses increase in the process of quench propagation. In addition, the high axial background fields can directly lead to higher peak hoop and radial tensile stresses in the superconducting layers.

In order to qualitatively clarify the effects of the external field on the stress distribution, the profiles of radial and hoop stresses in the middle point of the superconducting layers at the moment of $T_{\rm hot} = 200\,{\rm K}$ are plotted in Fig. 10, in which the stress distribution is approximately uniform along the tape width.

It is found from Fig. 10 that both the hoop and radial stresses increase with increasing the background field. With the background field from 0 T to 5 T and then to 10 T, the peak tensile radial stress rises from 1.69 MPa to 5.63 MPa and then to 9.7 MPa, and the corresponding peak tensile hoop stress climbs from 43 MPa to 207 MPa and then to 370 MPa. As a consequence of the low transverse quench propagation, the radial and hoop stresses vary greatly with increasing the radius at the nearby of the heat region due to the high temperature gradient and temperature rise. Except for several superconducting layers near the heat region, the remained ones are subjected to the tensile hoop stress. The maximum tensile radial and hoop stresses are located at the superconducting layer on the left side of the heat region and the innermost superconducting layer, respectively. In addition, the maximum tensile radial stress of 9.7 MPa at the 10 T background field case is close to the critical transverse tensile stress of about 10 MPa reported in Ref. [45]. It indicates that the separation between the constituent layers of the local tape may occur and hence the local tape could be damaged.

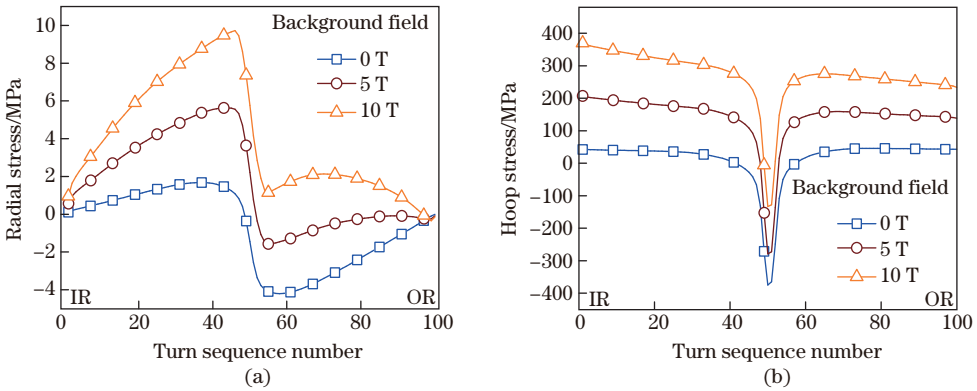

Fig. 10 Profiles of (a) the radial stress σ_r and (b) the hoop stress σ_φ in all superconducting layers at the moment of $T_{\rm hot} = 200\,{\rm K}$, where the turn sequence number is arranged from the innermost superconducting layer to the outermost superconducting layer (color online)

4.3 Effects of the coil size on the stress-strain states

The variation of the coil size may significantly affect the distributions of the stress and strain in coils. Here, we focus on the effects of the coil inner radius on the stress-strain state in the superconducting layers at the 10 T background field case. Figure 11 gives the profiles of the radial stress, hoop stress, and hoop strain in the superconducting layers at the moment of $T_{\rm hot} = 200\,{\rm K}$ with the normalized operating current of 0.6 and the coil inner radii of 10 mm, 20 mm, and 30 mm.

From Fig. 11(a), it is clear that the tensile radial stress in the superconducting layers descends with increasing the coil inner radius. The maximum tensile radial stress decreases from 15 MPa to 9.7 MPa with the coil inner radius from 10 mm to 30 mm. It can be concluded that increasing the coil inner radius can effectively suppress the maximum tensile radial stress, though the effect is limited.

In contrast to the variations of the radial stress, the hoop stress and strain ascend with increasing the coil inner radius, as shown in Figs. 11(b) and 11(c). The peak tensile hoop stress climbs from 180 MPa to 370 MPa with the coil inner radius from 10 mm to 30 mm, and the corresponding peak tensile hoop strain rises from 0.11% to 0.23%. This is easy to understand

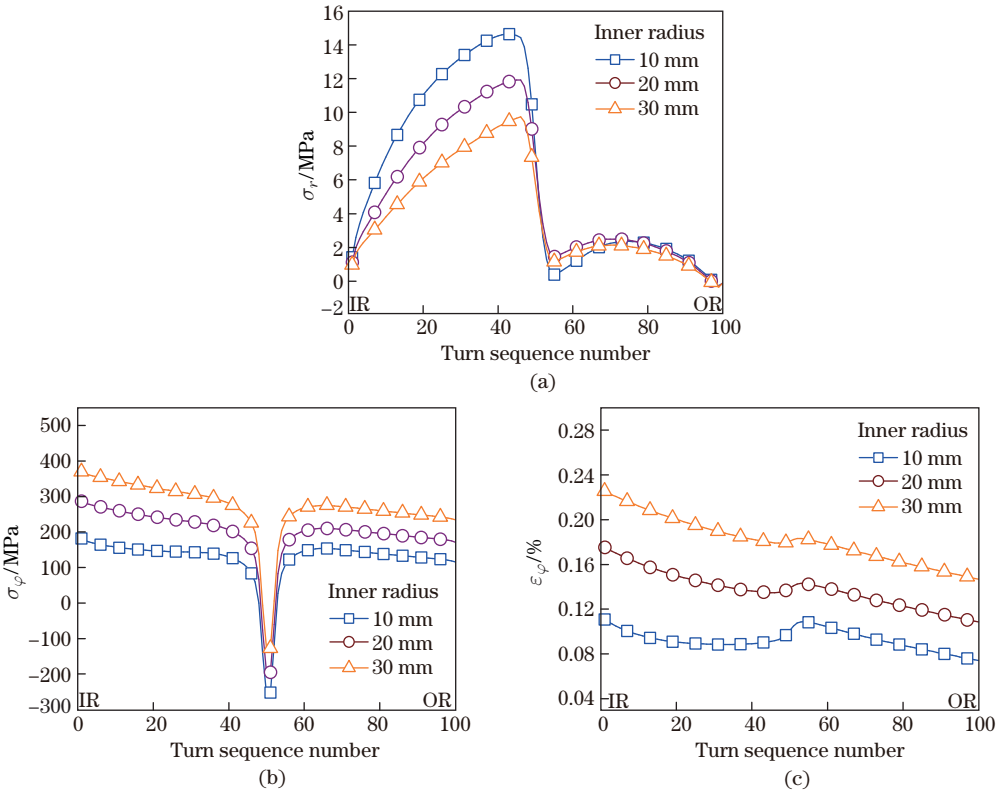

Fig. 11 Profiles of (a) the radial stress σ_r, (b) the hoop stress σ_φ, and (c) the hoop strain ε_φ in all superconducting layers along the radial direction at the moment of $T_{\rm hot} = 200\,{\rm K}$ (color online)

with the aid of the classic formula

$$\sigma_\varphi = rJ_\varphi B_z.$$

When the radius increases, the hoop stress should increase, even though the thermal stress is not considered in the simple formula.

5 Conclusions

In this paper, the 2D electro-magneto-thermal model and the elastoplastic mechanical model are used to study the quench and mechanical behaviors in REBCO pancake coils. The effects of several factors including the substrate materials, background field, and coil size are analyzed. The results are summarized as follows.

(i) When the transporting current increases, $E_{\rm MQ}$ of REBCO pancake coils descends and $V_{\rm NZP}$ in the transverse direction ascends. Stainless steel-based coil is found to have a higher $E_{\rm MQ}$ than Hastelloy-based coil, while the $V_{\rm NZP}$ of the former is lower. When the axial background field exceeds 2.5 T, $E_{\rm MQ}$ and $V_{\rm NZP}$ of the pancake coil slightly decrease with increasing the axial background field. In addition, the transverse $V_{\rm NZP}$ is insensitive to the variation of the coil size, while $E_{\rm MQ}$ increases with increasing the coil inner radius.

(ii) The radial strain evolutions can reflect the transverse quench propagation of REBCO coils.

(iii) The tensile hoop and radial stresses in the superconducting layers increase with the quench propagation. High background field can significantly increase the hoop and radial

stresses in quench coils. At the axial background field of 10 T, the maximum tensile radial stress in the superconducting layers at the moment of $T_{\rm hot} = 200$ K is close to the critical transverse stress, the possible delamination between the constituent layers may occur, and coils may be damaged in part.

References

[1] HAHN, S., KIM, K., KIM, K., HU, X. B., PAINTER, T., DIXON, I., KIM, S., BHATTARAI, K. R., NOGUCHI, S., JAROSZYNSKI, J., and LARBALESTIER, D. C. 45.5-tesla direct-current magnetic field generated with a high-temperature superconducting magnet. *nature*, **570**, 496–499 (2019)

[2] TSUKAMOTO, O., FUJIMOTO, Y., and TAKAO, T. Study on stabilization and quench protection of coils wound of HTS coated conductors considering quench origins — proposal of criteria for stabilization and quench protection. *Cryogenics*, **63**, 148–154 (2014)

[3] WEIJERS, H. W., MARKIEWICZ, W. D., GAVRILIN, A. V., VORAN, A. J., VIOUCHKOV, Y. L., GUNDLACH, S. R., NOYES, P. D., ABRAIMOV, D. V., BAI, H. Y., HANNAHS, S. T., and MURPHY, T. P. Progress in the development and construction of a 32 T superconducting magnet. *IEEE Transactions on Applied Superconductivity*, **26**, 4300807 (2016)

[4] TAKAHASHI, S., SUETOMI, Y., TAKAO, T., YANAGISAWA, Y., MAEDA, H., TAKEDA, Y., and SHIMOYAMA, J. I. Hoop stress modification, stress hysteresis and degradation of a REBCO coil due to the screening current under external magnetic field cycling. *IEEE Transactions on Applied Superconductivity*, **30**, 4602607 (2020)

[5] SUMPTION, M. D., MAJOROS, M., SUSNER, M., LYONS, D., PENG, X., CLARK, C. F., LAWLESS, W. N., and COLLINGS, E. W. Thermal diffusion and quench propagation in YBCO pancake coils wound with ZnO and mylar insulations. *Superconductor Science and Technology*, **23**, 075004 (2010)

[6] LIU, L. Y., CHEN, Y., ZHANG, H. Y., CHEN, W., SHI, J. T., YANG, X. S., ZHANG, Y., and ZHANG, Y. Quench characteristics comparison between solid nitrogen and conduction cooled REBCO coil under thermal disturbance and over current pulse. *IEEE Transactions on Applied Superconductivity*, **28**, 4603705 (2018)

[7] ZHANG, M., MATSUDA, K., and COOMBS, T. A. New application of temperature-dependent modelling of high temperature superconductors: quench propagation and pulse magnetization. *Journal of Applied Physics*, **112**, 043912 (2012)

[8] HAHN, S., PARK, D. K., BASCUNAN, J., and IWASA, Y. HTS pancake coils without turn-to-turn insulation. *IEEE Transactions on Applied Superconductivity*, **21**, 1592–1595 (2011)

[9] SHIN, H. J., KIM, K. L., CHOI, Y. H., YANG, D., KIM, Y. G., and LEE, H. A study on normal zone propagation behavior of partially insulated GdBCO coil. *IEEE Transactions on Applied Superconductivity*, **25**, 6600404 (2015)

[10] LECREVISSE, T., BADEL, A., BENKEL, T., CHAUD, X., FAZILLEAU, P., and TIXADOR, P. Metal-as-insulation variant of no-insulation HTS winding technique: pancake tests under high background magnetic field and high current at 4.2 K. *Superconductor Science and Technology*, **31**, 055008 (2018)

[11] WANG, Y. W., ZHENG, J. X., ZHU, Z. X., ZHANG, M., and YUAN, W. J. Quench behavior of high-temperature superconductor (RE)$Ba_2Cu_3O_x$ CORC cable. *Journal of Physics D*: *Applied Physics*, **52**, 345303 (2019)

[12] PI, W., LIU, Z. Q., LI, G. Q., MA, S. W., MENG, Y. R., SHI, Q. M., DONG, J., and WANG, Y. S. 4D simulation of quench behavior in quasi-isotropic superconducting cable of stacked REBCO tapes considering thermal contact resistance. *Superconductor Science and Technology*, **33**, 084005 (2020)

[13] SU, X. Y., LIU, C., ZHOU, J., ZHANG, X. Y., and ZHOU, Y. H. A method to access the electromechanical properties of superconducting thin film under uniaxial compression. *Acta Mechanica Sinica*, **36**, 1046–1050 (2020)

[14] BARTH, C., MONDONICO, G., and SENATORE, C. Electro-mechanical properties of REBCO coated conductors from various industrial manufacturers at 77 K, self-field and 4.2 K, 19 T. *Superconductor Science and Technology*, **28**, 045011 (2015)

[15] ZHANG, X. Y., SUN, C., LIU, C., and ZHOU, Y. H. A standardized measurement method and data analysis for the delamination strengths of YBCO coated conductors. *Superconductor Science and Technology*, **33**, 035005 (2020)

[16] WANG, T. G., LI, Z. X., GAO, J. J., and GOU, X. F. Mechanical damage of $YBa_2Cu_3O_7$ coated conducting films caused by its CeO_2 interface with defect. *International Journal of Applied Mechanics*, **11**, 1950038 (2019)

[17] GRAY, W. H. and BALLOU, J. K. Finite element stress analysis of orthotropic solenoids. *Journal of Applied Physics*, **48**, 3100–3109 (1977)

[18] ARP, V. Stresses in superconducting solenoids. *Journal of Applied Physics*, **48**, 2026–2036 (1977)

[19] WANG, L., WANG, Q. L., LI, L. K., QIN, L., LIU, J. H., LI, Y., and HU, X. N. The effect of winding conditions on the stress distribution in a 10.7 T REBCO insert for the 25.7 T superconducting magnet. *IEEE Transactions on Applied Superconductivity*, **28**, 4600805 (2018)

[20] LIU, D. H., ZHANG, W. W., YONG, H. D., and ZHOU, Y. H. Thermal stability and mechanical behavior in no-insulation high-temperature superconducting pancake coils. *Superconductor Science and Technology*, **31**, 085010 (2018)

[21] LIU, D. H., ZHANG, W. W., YONG, H. D., and ZHOU, Y. H. Numerical analysis of thermal stability and mechanical response in a no-insulation high-temperature superconducting layer-wound coil. *Superconductor Science and Technology*, **32**, 044001 (2019)

[22] XIA, J., BAI, H. Y., YONG, H. D., WEIJERS, H. W., PAINTER, T. A., and BIRD, M. D. Stress and strain analysis of a REBCO high field coil based on the distribution of shielding current. *Superconductor Science and Technology*, **32**, 095005 (2019)

[23] HONG, Z. Y., CAMPBELL, A. M., and COOMBS, T. A. Numerical solution of critical state in superconductivity by finite element software. *Superconductor Science and Technology*, **19**, 1246–1252 (2006)

[24] COMSOL Co., Ltd. *COMSOL Multiphysics Material Library*, Beijing (2020)

[25] LU, J., CHOI, E. S., and ZHOU, H. D. Physical properties of Hastelloy C-276 at cryogenic temperatures. *Journal of Applied Physics*, **103**, 064908 (2008)

[26] CHAN, W. K. and SCHWARTZ, J. Improved stability, magnetic field preservation and recovery speed in $(Re)Ba_2Cu_3O_x$-based no-insulation magnets via a graded-resistance approach. *Superconductor Science and Technology*, **30**, 074007 (2017)

[27] XU, A., JAROSZYNSKI, J. J., KAMETANI, F., CHEN, Z., LARBALESTIER, D. C., VIOUCHKOV, Y. L., CHEN, Y., XIE, Y., and SELVAMANICKAM, V. Angular dependence of J_c for YBCO coated conductors at low temperature and very high magnetic fields. *Superconductor Science and Technology*, **23**, 014003 (2010)

[28] DURON, J., GRILLI, F., DUTOIT, B., and STAVREV, S. Modelling the E-J relation of high-T_c superconductors in an arbitrary current range. *Physica C*: *Superconductivity*, **401**, 231–235 (2004)

[29] IKEBE, M., FUJISHIRO, H., NAITO, T., NOTO, K., KOHAYASHI, S., and YOSHIZAWA, S. Thermal conductivity of YBCO(123) and YBCO(211) mixed crystals prepared by MMTG. *Cryogenics*, **34**, 57–61 (1994)

[30] PHILLIPS, N. E. and FISHER, R. A. The specific heat of high-T_c superconductors. *Progress in Low Temperature Physics*, Elsevier, Amsterdam, 267–357 (1992)

[31] National Institute of Standards and Technology. *Cryogenic Technology Resources*, NIST, Gaithersburg (2020) http://cryogenics.nist.gov

[32] KIM, N. H. *Introduction to Nonlinear Finite Element Analysis*, Springer Science+Business Media, New York, 265–366 (2015)

[33] GAO, P. F., CHAN, W. K., WANG, X. Z., ZHOU, Y. H., and SCHWARTZ, J. Stress, strain and electromechanical analyses of $(RE)Ba_2Cu_3O_x$ conductors using three-dimensional/two-dimensional mixeddimensional modeling: fabrication, cooling and tensile behavior. *Superconductor Science and Technology*, **33**, 044015 (2020)

[34] MIYAZAKI, H., IWAI, S., TOSAKA, T., TASAKI, K., and ISHII, Y. Delamination strengths of different types of REBCO-coated conductors and method for reducing radial thermal stresses of impregnated REBCO pancake coils. *IEEE Transactions on Applied Superconductivity*, **25**, 6602305 (2015)

[35] FUJISHIRO, H., AINSLIE, M., TAKAHASHI, K., NAITO, T., YANAGI, Y., ITOH, Y., and NAKAMURA, T. Simulation studies of mechanical stresses in REBaCuO superconducting ring bulks with infinite and finite height reinforced by metal ring during field-cooled magnetization. *Superconductor Science and Technology*, **30**, 085008 (2017)

[36] OSAMURA, K., SUGANO, M., MACHIYA, S., ADACHI, H., OCHIAI, S., and SATO, M. Internal residual strain and critical current maximum of a surrounded Cu stabilized YBCO coated conductor. *Superconductor Science and Technology*, **22**, 065001 (2009)

[37] ALLEN, N. C., CHIESA, L., and TAKAYASU, M. Structural modeling of HTS tapes and cables. *Cryogenics*, **80**, 405–418 (2016)

[38] MIYAGI, D., KATO, M., YOSHIDA, Y., and TSUDA, M. Influence of a coil bobbin on transient thermal stress in a REBCO pancake coil. *IEEE Transactions on Applied Superconductivity*, **28**, 4603505 (2018)

[39] ZERMENO, V., SIROIS, F., TAKAYASU, M., VOJENCIAK, M., KARIO, A., and GRILLI, F. A self-consistent model for estimating the critical current of superconducting devices. *Superconductor Science and Technology*, **28**, 085004 (2015)

[40] NIU, M. D., YONG, H. D., XIA, J., and ZHOU, Y. H. The effects of ferromagnetic disks on AC losses in HTS pancake coils with nonmagnetic and magnetic substrates. *Journal of Superconductivity and Novel Magnetism*, **32**, 499–510 (2019)

[41] SHIROYANAGI, Y., SAMPSON, W. B., and GHOSH, A. K. Quench propagation studies using a small bifilar YBCO coil. *AIP Conference Proceedings*, **58**, 265–272 (2012)

[42] WANG, X. Z., GUAN, M. Z., and MA, L. Z. Strain-based quench detection for a solenoid superconducting magnet. *Superconductor Science and Technology*, **25**, 095009 (2012)

[43] TONG, Y. J., GUAN, M. Z., and WANG, X. Z. Theoretical estimation of quench occurrence and propagation based on generalized thermoelasticity for LTS/HTS tapes triggered by a spot heater. *Superconductor Science and Technology*, **30**, 045002 (2017)

[44] MARINUCCI, C., BOTTURA, L., CALVI, M., and WESCHE, R. Quench analysis of a high-current forced-fow HTS conductor model for fusion magnets. *IEEE Transactions on Applied Superconductivity*, **21**, 2445–2448 (2011)

[45] VAN DER LAAN, D. C., EKIN, J. W., CLICKNER, C. C., and STAUFFER, T. C. Delamination strength of YBCO coated conductors under transverse tensile stress. *Superconductor Science and Technology*, **20**, 765–770 (2007)